

Study of the Reactions of O^- with CF_4 and CHF_3 by Ab Initio Calculations

Mitsuo Yamamoto,* Koichi Yamashita, and Masayoshi Sadakata

Department of Chemical System Engineering, The University of Tokyo, 7-3-1 Hongo, Bunkyo-ku, Tokyo 113-8656

(Received December 21, 2001)

Previous experiments on the reactions of O^- with CF_4 and CHF_3 using a selected ion flow tube (SIFT) have indicated that many species, such as CF_3^-, F^-, and HF_2^-, are produced in the $O^- + CHF_3$ reaction, although no reaction proceeds in the $O^- + CF_4$ reaction under thermal conditions. Ab initio molecular orbital calculations were carried out in this study to clarify the reason for the difference in the reactivity between these two reactions. Potential energy surfaces (PESs) for the possible reaction channels were computed at the UMP2/6-31+G** level. Although the S_N2-type reactions, such as the $CF_3O^- + F$ channel, are exothermic, the calculated activation energy for the $O^- + CF_4$ reaction is rather high, 222 kJ/mol. The energies of the transition states in the $O^- + CHF_3$ reaction are below that of the reactant. We may conclude that the difference in reactivity between the two reactions is attributable to the charge distribution of each molecule. The H atom in CHF_3 has a large effect on increasing the reactivity because the positively charged H atom attracts O^-, whereas O^- has difficulty approaching the CF_4 molecule because of the four negatively charged F atoms.

Perfluorocompounds (PFCs) have received considerable attention in recent years because they are greenhouse gases specified as regulated gases in the third session of the Conference of the Parties on Climate Change (COP3). Studies on their decomposition, such as combustion,[1] catalytic method[2] and the plasma discharge method,[3,4] have been performed in recent years, while kinetic studies of relevant gas-phase reactions involving PFCs are important for understanding their mechanisms and their fate in the atmosphere. The chemistry of radical reactions and ion–molecule reactions in the atmosphere has been studied in atmospheric chemistry.[5] It has been recognized that ion–molecule reactions involving negative ions have significant roles in the atmosphere.[6]

Kinetic studies of ion–molecule reactions have utilized various methods, such as a selected ion flow tube (SIFT)[7] and guided ion beam methods.[8] Some reactions of O^- and O_2^- with PFCs, hydrofluorocarbons (HFCs) and related compounds have been studied by using a SIFT method.[9–11] Morris[12] measured the rate coefficients and branching ratios for the reactions of O^- and O_2^- with CF_4, CF_3Cl, CF_3Br, CF_3I and C_2F_4 at 298 and 500 K. Mayhew[13] also investigated the reactivity of O^- and O_2^- with some halogenated methanes, including CF_4. Both Morris and Mayhew concluded that the reaction of O^- and CF_4 would not proceed at all under thermal conditions. On the other hand, Peverall et al.[14] measured the rate coefficients and branching ratios for the reactions of O^- and O_2^- with $CHCl_2F$, $CHClF_2$, CHF_3, CH_2ClF, CH_2F_2, CH_3F, CHF_2CHF_2, CH_2FCF_3, and CH_3CHF_2 at 300 K and 0.5 Torr using a SIFT method. They concluded that the reaction of O^- with CHF_3 proceeds relatively easily with a reaction rate coefficient of 1.9×10^{-9} cm^3 molecule^{-1} s^{-1} and with the produced ions being e^- (30%), OH^- (4%), F^- (16%), HF_2^- (3%), and CF_3^- (47%). These results are very interesting because the structure of CHF_3 is similar to that of CF_4, except that an F atom is replaced with an H atom.

The reactions of neutral radical species, such as $O(^1D)$, $O(^3P)$, and OH, with hydrofluorocarbons by ab initio or density functional theory (DFT) methods have been investigated. Wang et al.[15] evaluated the difference in the reaction between $O(^3P)$ with CH_3F and $O(^3P)$ with CH_2F_2, which occurs via direct hydrogen abstraction. They optimized the geometries of the reactants, the transition state and the products at the UMP2(full)/cc-pVDZ level, and obtained the total energies via the G2(MP2) scheme. The reactions of $O(^3P) + CH_3F$, CH_2F_2 were compared with the $O(^3P) + CH_4$, CHF_3 reactions. Wang et al. also investigated the reaction of $NH(X^3\Sigma^-)$ with CH_xF_{4-x} (x = 1, 2, 3, 4)[16] via direct hydrogen abstraction mechanisms. The potential energy surfaces (PESs) were calculated at the G2(MP2) level and the effect of fluorine substitution was studied.

The dynamics of the gas-phase reactions of ions with methane, chloromethanes or fluoromethanes were also investigated.[17–20] Even though there have been many studies of S_N2-type reactions,[21,22] there have only been a few studies on the reactions of O^- with molecules. Viggiano et al.[23] studied the $O^- + CH_4$ reaction using a selected ion flow drift tube and a theoretical method at the QCISD(T) level of theory. Lee et al. investigated the reaction of O^- with CH_2F_2 with ab initio molecular orbital calculations[24] and compared their results with the experimental results.[25] In this study, the calculations were carried out at various levels of sophistication, such as MP2/6-31++G**//MP2/6-31++G** and MP4(SDTQ)/6-31++G(2df,p)//MP2/6-31++G**, to investigate the reaction paths and the relative energies of the possible reaction channels. Lee et al. also evaluated the reactivity of OH^- with CH_2F_2 by experiment and ab initio calculations[26] and compared the reactivity of OH^- with O^-.

According to experimental[14] and theoretical[24] studies, three

kinds of reaction channels can be considered in the reaction of O^- with hydrofluorocarbons: S_N2 type, H abstraction and H_2 abstraction channels. The main purpose of the present study is to explain the difference in the reactivity between the O^- + CF_4 and the O^- + CHF_3 reactions by examining three possible reaction paths using ab initio molecular orbital calculations.

Computational Methods

All calculations were performed with the Gaussian 98 program.[27] All structures were optimized at the MP2 level with the 6-31+G** basis set. The reaction enthalpies of the possible reaction channels were computed at different levels of theory and different basis sets, and were compared with experimental values in order to evaluate the appropriateness of the level of theory and the basis sets used in the calculations. We chose the reaction of O^- with CHF_3 in evaluating the appropriateness of our calculations, since there are several reaction channels for a comparison. All of the calculations of reaction enthalpies were performed at the MP2/6-31+G**, MP4-(SDTQ)/6-31+G**, MP4(SDTQ)/6-31++G(2df,p), and MP4-(SDTQ)/6-311++G(2df,p) levels.

1. The Reaction of O^- with CF_4. The PESs of the O^- + CF_4 reaction were investigated by assuming that the reaction proceeds as an S_N2-type reaction, and only exothermic reaction channels were calculated. The reaction channels considered in our study are as follows:

$$O^- + CF_4 \rightarrow CF_3O^- + F \quad (1)$$

$$\rightarrow F^- + CF_3O \quad (2)$$

$$\rightarrow F_2{}^- + CF_2O \quad (3)$$

$$\rightarrow CF_2O^- + F_2 \quad (4)$$

$$\rightarrow CF_3{}^- + OF \quad (5)$$

$$\rightarrow OF^- + CF_3 \quad (6)$$

The reaction enthalpies of reactions (1)–(6), estimated by using the experimental NIST data,[28] are given in Table 1. Because there are no enthalpy data for CF_3O and CF_2O in the NIST database, the theoretical values at 298.15 K and 1 atm at the MP4(SDTQ)/ 6-311++G(2df,p)//MP2/6-31+G* are also included in Table 1. The validity of the calculated values is discussed in the reaction enthalpies section.

Reactions (1)–(4) are expected to proceed as S_N2-type reactions. O^- attacks the carbon atom nucleophilically. On the other hand, reactions (5) and (6) proceed by a nucleophilic attack on the F atom. We investigated reactions (1)–(3) because these reaction channels are exothermic reactions and reactions (4)–(6) are relatively high endothermic reactions.

Table 1. Reaction Enthalpies (in kJ/mol) of the Reaction of O^- with CF_4

Channels	Expt[20]	MP4(SDTQ)/6-311++G(2df,p) //MP2/6-31+G*(298.15 K,1 atm)
1) CF_3O^- + F	−158 ± 30	−181.0
2) F^- + CF_3O	—	−56.6
3) $F_2{}^-$ + CF_2O	−108 ± 28	−80.1
4) CF_2O^- + F_2	—	+290.5
5) $CF_3{}^-$ + OF	+284 ± 39	+308.2
6) OF^- + CF_3	+241 ± 30	+255.2

2. The Reaction of O^- with CHF_3. PESs of the O^- + CHF_3 reaction were calculated, and it was predicted that the reaction proceeds in two reaction channels, S_N2 type and H abstraction channels. The produced ions and their percentage ratios of the O^- + CHF_3 reaction are: e^- (30%), OH^- (4%), F^- (16%), $HF_2{}^-$ (3%), and $CF_3{}^-$ (47%).[14] F^-, $HF_2{}^-$, and electrons are considered to be produced from the following reaction channels, which can be specified as S_N2-type reactions:

(i) $O^- + CHF_3 \rightarrow HF + COF_2{}^- \rightarrow HF + F^- + COF$

(ii) $\rightarrow HF_2{}^- + COF \rightarrow F^- + HF + COF$

(iii) $\rightarrow HF + COF_2{}^- \rightarrow HF + COF_2 + e^-$

It is difficult for F^-, HF, and COF to be produced directly by the collision of O^- and CHF_3. Two reaction channels for producing F^- are possible. One way is that HF and $COF_2{}^-$ are produced as intermediate products and F^- is produced from $COF_2{}^-$ (reaction channel (i)). The other way is that $HF_2{}^-$ and COF are produced as intermediate products (reaction channel (ii)). Electrons are expected to be produced by electron detachment from $COF_2{}^-$.[14] It is possible that $CF_3{}^-$ and OH^- are produced through H abstraction by O^-.

Results and Discussion

1. Reaction Enthalpies. The reaction enthalpies for the O^- + CHF_3 reaction channels[14] calculated at MP2/6-31+G**, MP4(SDTQ)/6-31+G**//MP2/6-31+G**, MP4(SDTQ)/6-31++G(2df,p)//MP2/6-31+G**, and MP4(SDTQ)/6-311++G(2df,p)//MP2/6-31+G**, are shown in Table 2. ΔH implies the reaction enthalpy at 298.15 K and 1 atm. The MP2/6-31+G** frequencies were used for the ΔH calculations. The calculated values of the reaction enthalpies were improved slightly by changing the level of theory from MP2 to MP4 and the correlation effect has almost converged at the MP4 level. However, the differences in the calculated enthalpies between MP4 (SDTQ)/6-31+G** and MP4 (SDTQ)/6-31++G(2df,p) are relatively large. The MP4 (SDTQ)/6-31++G(2df,p) enthalpies are significantly improved and are close to the experimental values. Because the calculated values at MP4 (SDTQ)/6-311++G(2df,p) are almost the same as those at MP4 (SDTQ)/6-31++G(2df,p), the basis set has almost converged.

These reaction enthalpies indicate that the MP4 theory and the 6-311++G(2df,p) basis set is good enough to obtain reliable stationary point energies and that the MP2/6-31+G** level is suitable for structure optimizations. In this study, the MP2/6-31+G** level is utilized for structure optimization.

2. The O^- + CF_4 Reaction. 2.1 O^- + $CF_4 \rightarrow CF_3O^-$ + F, F^- + CF_3O. The CF_3O^- + F and F^- + CF_3O channels proceed as typical S_N2-type reactions. In both reaction channels, O^- attacks carbon through the F_3 triangle of the CF_4 molecules at the initial step. Unrestricted spin wavefunctions

Table 2. Calculated Reaction Enthalpies (in kJ/mol) for Several Reactions

Channels		MP2/6-31+G**	MP4(SDTQ) /6-31+G**	MP4(SDTQ) /6-31++G(2df,p)	MP4(SDTQ) /6-311++G(2df,p)	Expt[14]	Expt[28]
$F^- + HF + COF$	ΔE	−154.7	−159.5	−132.9	−124.9	—	—
	ΔH	−166.3	−152.0	−125.4	−117.4	−110	−106 ± 10
$HF + COF_2^-$	ΔE	−320.4	−323.2	−299.7	−301.9	—	—
	ΔH	−332.0	−313.8	−290.3	−292.5	—	—
$HF_2^- + COF$	ΔE	−349.1	−350.6	−320.3	−319.9	—	—
	ΔH	−360.7	−341.5	−310.2	−310.8	−271	−296 ± 8
$e^- + HF + COF_2$	ΔE	−321.9	−318.9	−311.2	−316.7	—	—
	ΔH	−333.5	−330.5	−322.8	−328.3	−326	−323
$CF_3^- + OH$	ΔE	−32.6	−59.8	−23.3	−24.2	—	—
	ΔH	−23.1	−50.4	−13.8	−14.7	−22 ± 14	−23 ± 19
$OH^- + CF_3$	ΔE	−25.4	−24.2	−16.4	−17.5	—	—
	ΔH	−16.8	−15.6	−7.8	−9.0	−10 ± 8	−19 ± 2

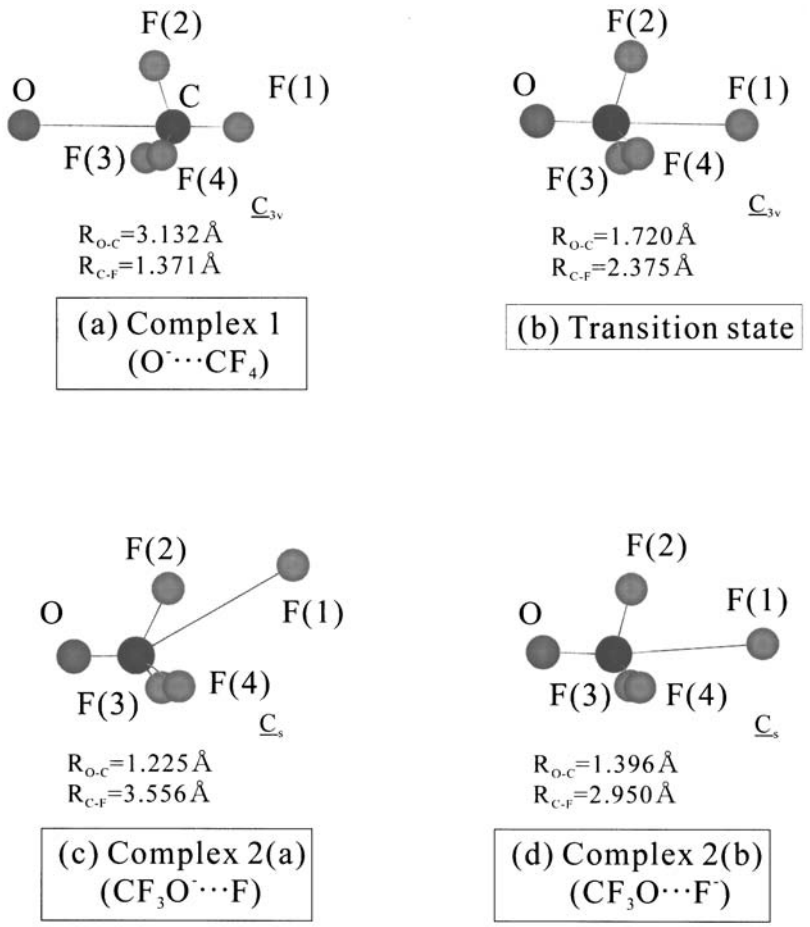

Fig. 1. Optimized structures of (a) complex 1, (b) transition state, (c) complex 2(a), and (d) complex 2(b) of the CF_3O^- + F channel.

(UMP2/6-31+G**) were used throughout the PES calculations of the $O^- + CF_4$ reaction. The spin contamination was found to be small in the computed wave functions. The range of $<S^2>$ was from 0.75 to 0.76.

As O^- approaches the carbon atom, the bond length between the C atom and the F atom gradually becomes longer. When the C–O distance is 3.13 Å, a complex ($O^-\cdots CF_4$) with C_{3v} symmetry (Fig. 1(a)) was optimized at a stationary point. The reaction proceeds on the $O^-\cdots CF_4$ surface within C_{3v} symmetry and the total energy gradually increases. The transition state structure shown in Fig. 1(b) was optimized within C_{3v} symmetry. The energy of the transition state is rather high and the activation energy calculated for this reaction is 221.9 kJ/mol.

Two complexes were optimized. One complex, defined as complex 2(a) with C_S symmetry (Fig. 1(c)), $CF_3O^-\cdots F$, is on

the CF_3O^- + F channel. The other, defined as complex 2(b) with C_S symmetry (Fig. 1(d)), $CF_3O\cdots F^-$, is on the F^- + CF_3O channel. Morris et al.[29] theoretically investigated CF_3O and CF_3O^-, and found that CF_3O ($^2A'$) has a Jahn–Teller distorted C_S symmetry structure, while CF_3O^-($^1A_1$) has a C_{3v} symmetry structure. The C_S-symmetry $CF_3O^-\cdots F$ structure is Jahn–Teller distorted by the existence of the F(1) atom. Because CF_3O prefers a Jahn–Teller distorted C_S-symmetry, complex 2(b) with the spherical $F(1)^-$ prefers a C_S symmetry structure. Therefore, complexes 2(a) and 2(b) with C_S symmetry are considered to be produced by a Jahn–Teller distortion along the C_{3v} symmetry reaction path. We have not actually traced the PES between these complexes and the transition state by intrinsic reaction coordinate (IRC) calculations, since it is necessary to take into account the vibronic interaction to produce the Jahn–Teller distorted reaction paths.

Comparing complex 2(a) with complex 2(b), some differences are apparent. In the case of complex 2(a), the distance of C–F(1) is relatively large, 3.56 Å, and the angle of O–C–F(1) is strongly bent (∠OCF(1) = 151.4°). On the other hand, the distance of C–F(1) in complex 2(b) is 2.95 Å and the O–C length is 0.17 Å longer than that in complex 2(a). The angle OCF(1) is 174.3°. The energy of the $CF_3O^-\cdots F$ structure is 114.6 kJ/mol more stable than that of $CF_3O\cdots F^-$; $CF_3O\cdots F^-$ corresponds to the exited state of that of $CF_3O^-\cdots F$. Therefore, complex 2(a) may be connected to the transition state adiabatically, and there should be a corresponding path of the excited state for complex 2(b). These two paths are plotted by the dotted lines in Fig. 4. After the formation of complex 2(a) and complex 2(b), the reactions proceed to the CF_3O^- + F channel and the F^- + CF_3O channel, respectively.

2.2 O^- + CF_4 → F_2^- + CF_2O. The PES of the F_2^- + CF_2O reaction channel is difficult to predict. However, this reaction channel is expected to proceed as an S_N2-type reaction, because there are only two reaction types, a nucleophilic attack on carbon and a nucleophilic attack on fluorine, and O^- cannot get close to negatively charged F atoms under thermal conditions. Taking the geometry of complex 2(a) into consideration, the F(1) atom exists relatively near to the F(2) atom. In order to calculate the PES of the F_2^- + CF_2O channel, the C–F(2) distance was gradually changed and the geometry was optimized in each 0.05 Å step. Figure 2 shows the optimized geometry and the atomic charge distribution when the C–F(2) distance is 2.44 Å. This geometry consists of two parts, F_2^--like and CF_2O-like geometries. The total atomic charge of F(1) and F(2) is −0.96 and the distance is 1.79 Å; this geometry is therefore similar to the F_2^- geometry shown in Fig. 3(b), although the distance between the F atoms is a little shorter. As for the geometry of OCF(3)F(4), the bond lengths are almost the same as those of CF_2O shown in Fig. 3(a), and the angles of OCF(3) and OCF(4) are only 3° smaller than those of CF_2O. Thus, the intermediate shown in Fig. 2 is considered to be on the side of the F_2^- + CF_2O channel. On the other hand, F_2^- and CF_2O were not produced by scanning the C–F(2) distance of complex 2(b).

According to the above observations, it may be concluded that F_2^- and CF_2O are produced from the surface of complex 2(a) ($CF_3O^-\cdots F$).

2.3 Summary of the O^- + CF_4 Reaction. A schematic diagram of the O^- + CF_4 reaction computed at the UMP2/6-31+G** level is shown in Fig. 4, and the energies relative to the O^- + CF_4 of some stationary points are listed in Table 3. As explained above, there is one transition state in this reaction and the reaction barrier is rather high. Two product-like complexes exist between the transition state and the products. One has $CF_3O\cdots F^-$ geometry with C_S symmetry on the surface of the F^- + CF_3O production channel. The other is in the CF_3O^-

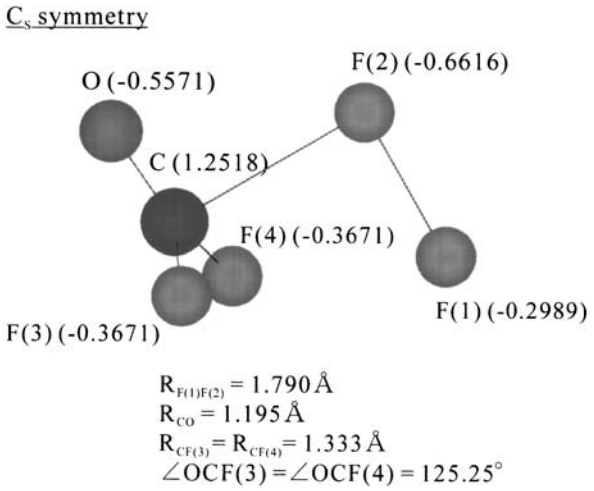

Fig. 2. Geometry and atomic distribution scanned on the surface of the $F_2^-\cdots CF_2O$ channel ($R_{CF(2)}$ = 2.44 Å).

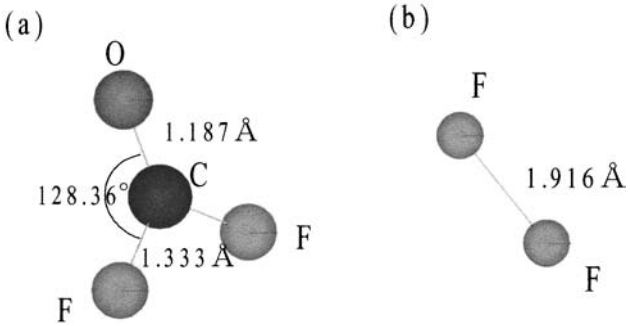

Fig. 3. Geometries of (a) CF_2O and (b) F_2^- calculated at the MP2/6-31+G** level.

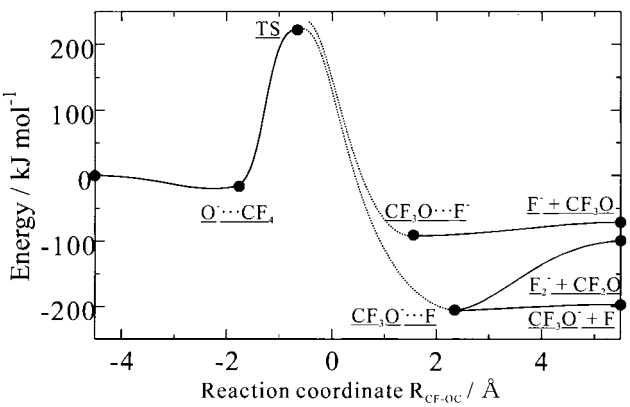

Fig. 4. Schematic diagram of the O^- + CF_4 reaction calculated at the UMP2/6-31+G** level.

Table 3. Energies Relative to $O^- + CF_4$ (in kJ/mol) of Some Stationary Points Calculated at the UMP2/6-31+G** Level

Species	ΔE
$O^- + CF_4$	0.0
$O^-\cdots CF_4$ (complex 1)	−16.7
TS	221.9
$CF_3O^-\cdots F$ (complex 2(a))	−205.5
$CF_3O^- + F$	−197.5
$CF_3O\cdots F^-$ (complex 2(b))	−90.9
$F^- + CF_3O$	−71.6
$F_2^- + CF_2O$	−99.5

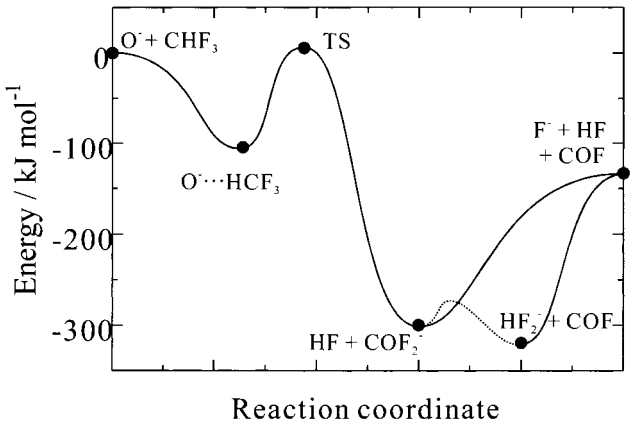

Fig. 5. Schematic diagram of the $F^- + HF + COF$ channels calculated at the UMP2/6-31+G** level.

+ F production channel. As the reaction proceeds from complex 2(a) on the surface of the $CF_3O^- + F$ channel, the reaction path is further separated into two channels, so that $F_2^- + CF_2O$ and $CF_3O^- + F$ are finally produced.

It is concluded that our calculations agree with the experimental results,[12,13] that it is difficult for the $O^- + CF_4$ reaction to proceed because of a high reaction barrier.

3. The Reaction of $O^- + CHF_3$. 3.1 $O^- + CHF_3 \rightarrow F^- + HF + COF$ (S_N2-Type Reaction). S_N2-type reactions are expected to proceed in accordance with reactions (i)–(iii) described in section 2 of Computational Methods. The PES of each reaction channel was calculated at the UMP2/6-31+G** level, and a schematic diagram of the $F^- + HF + COF$ channel is shown in Fig. 5. There is a reactant-like complex ($O^-\cdots HCF_3$) with C_S symmetry and a transition state with C_S symmetry. The energies relative to the $O^- + CHF_3$ of complex and transition state are listed in Table 4. Almost no reaction barrier exists in this reaction. As the reaction proceeds from the transition state, the reaction path is separated into two, the $HF + COF_2^-$ channel and the $HF_2^- + COF$ channel. Finally, $F^- + HF + COF$ is produced from both channels. These observations correspond to the prediction in section 2 of Computational Methods. The details of each reaction channel are described below.

Table 4. Energies Relative to $O^- + CHF_3$ (in kJ/mol) of Some Stationary Points Calculated at UMP2/6-31+G** Level

Reaction type	Species	ΔE
S_N2 type	$O^-\cdots HCF_3$ (complex)	−106.1
	Transition state	5.6
H abstraction	$O^-\cdots HCF_3$ (Complex 1)	−87.7
	$CF_3^-\cdots OH$ (Complex 2)	−108.4

< Reactant → Complex ($O^-\cdots CHF_3$) → Transition State > The geometry of the complex ($O^-\cdots CHF_3$) optimized at the UMP2/6-31+G** level is shown in Fig. 6(a), in which the electronic state is $^2A'$ with C_S symmetry. The optimized geometry was different from the expected one: ∠OCF(1) is not 180° and ∠OHC is 178.9°. This geometry with C_S symmetry indicates that O^- abstracts the H atom at the first step of the S_N2-type reaction. As the reaction further proceeds from the $O^-\cdots HCF_3$ structure, the CHF_3 molecule is gradually rotated and O^- attacks the C atom instead of the H atom. The transition state is optimized as shown in Fig. 6(b), in which the electronic state is $^2A'$ with C_S symmetry and ∠OCF(1) is 163.9°. As O^- comes close to the C atom, the C–F(1) bond length gradually increases and both ∠F(1)CF(2) and ∠F(1)CF(3) also become larger. The reaction barrier calculated at UMP2/6-31+G** is only 5.6 kJ/mol (endothermic). In the case of UMP4(SDTQ)/6-31++G(2df,p), the reaction barrier is −3.2 kJ/mol (exothermic). It may be concluded that no barrier exists in the S_N2-type reaction of O^- with CHF_3, which agrees with the experimental results.[14]

< Transition State → $HF + COF_2^-$ → $F^- + HF + COF$ > IRC calculations were carried out to connect the $O^-\cdots HCF_3$ geometry with the second complex of the $F^- + HF + COF$ channel. The IRC calculation indicates that the F(1) atom came apart from the C atom gradually as the reaction proceeds. However, because the H atom also came apart from the C atom and came near to the F(1) atom, the $HF\cdots COF_2^-$ geometry as in Fig. 7 was optimized in the final step. Figure 7 shows the geometry on the PES of $HF + COF_2^-$ when the C–F(1) bond length is 2.58 Å. The geometries of HF(1) and COF(2)F(3) are very similar to those geometries of the HF molecule and the

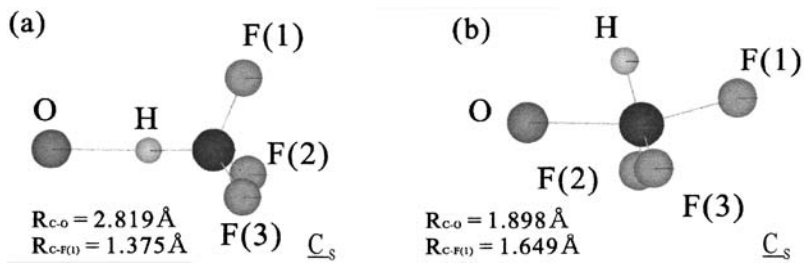

Fig. 6. Geometries of (a) complex and (b) transition state of the $F^- + HF + COF$ channel.

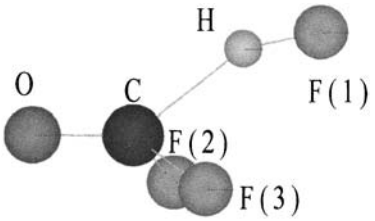

Fig. 7. Geometry scanned on the surface of the HF + COF_2^- channel.

COF_2^- anion, respectively. Furthermore, the charge of COF_2^- is almost minus one. These observations show that HF and COF_2^- are produced as the first products of the S_N2-type reaction.

In the next step, it was expected that COF_2^- divided into F^- and COF, with F^-, HF and COF being produced finally. As the F atom separates from the C atom in the COF_2^- structure, the residual COF geometry gradually changes to the COF molecule geometry and the energy on the PES continues to increase. The total energy of this structure and HF becomes close to that of F^- + HF + COF production.

$<$ **Transition State** $\rightarrow$ **HF_2^- + COF** $\rightarrow$ **F^- + HF + COF** $>$ At the dissociation regions of HF + COF_2^- and HF_2^- + COF, there may exist van der waals complexes, $COF_2^-\cdots$HF and $HF_2^-\cdots$COF. A transition state of the isomerization between $COF_2^-\cdots$HF and $HF_2^-\cdots$COF is considered to exist. We have not fully optimised the structures of these complexes and the transition state because this isomerization reaction would not be important for the main purpose of out study. Instead, the path is indicated by dotted line in Fig. 5.

Comparing the total energy of HF + COF_2^- with that of HF_2^- + COF, the latter products are approximately 20 kJ/mol more stable than the former ones. Figure 7 shows the geometry on the IRC with C_S symmetry. There is a possibility that the distance between an F atom, such as the F(2) atom in Fig. 7, and the C atom gradually increases. Even though C_S symmetry is lowered to C_1 symmetry, this change can occur from an energy point of view, and the geometry changed dramatically. Figure 8 shows the geometry ($R_{CF(2)}$ = 2.60 Å) on the PES of the HF_2^- + COF channel. This structure consists of two parts, the HF(1)F(2) part and the COF(3) part. Each geometry and the atomic charge distribution are similar to those of the HF_2^- and COF geometries. These observations indicate that HF_2^- and COF are produced by an S_N2-type reaction. After the production of HF_2^- and COF, F^- was produced from the HF_2^-

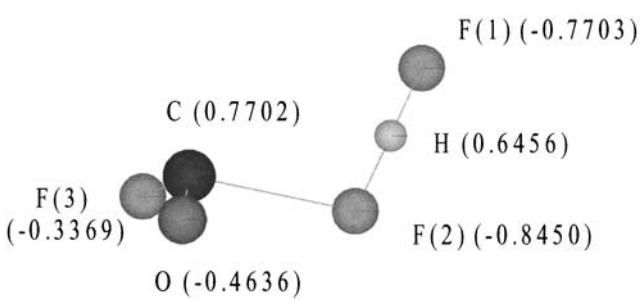

Fig. 8. Geometry scanned on the surface of the HF_2^- + COF channel.

Table 5. Electron Affinity of COF_2, CF_3, OH, and F Calculated at the MP4/6-311++G(2df,p) Level

Substances	Electron Affinity / kJ mol^{-1}
COF_2	−15.0
CF_3	162.7
OH	156.0
F	312.4

structure and the energy of this PES gradually increased until reaching the production of F^- + HF.

$<$ **HF + COF_2^- $\rightarrow$ e^- + HF + COF_2** $>$ Peverall et al. proposed that electrons are produced by the following reaction path:[14]

$$O^- + CHF_3 \rightarrow [HF\cdots COF_2]^{*-} \rightarrow e^- + HF + COF_2$$
$$\Delta H = -326 \text{ kJ/mol}$$

Lee et al. indicated that electron production by the O^- + CH_2F_2 reaction occurs by two routes, a temperature-dependent route and a temperature-independent route.[24] The temperature-dependent route implies that electrons are produced via the electron detachment of the product ion CF_2^-. The temperature-independent route implies that the electrons are produced via electron detachment of the product-like complex $H_2O\cdots CF_2^-$. As mentioned above concerning the present study, the reaction proceeds by a nucleophilic attack on carbon, and the reactant-like complex $O^-\cdots HCF_3$ and the transition state $OCHF_2\cdots F^-$ exist in the HF + COF_2^- channel. It is expected that electrons are produced only by a temperature-dependent route via electron detachment from COF_2^-.

In order to confirm the feasibility of this expectation, the electron affinity of COF_2 was calculated. Table 5 shows the electron affinity of COF_2 calculated at the UMP4/6-311++G(2df,p)//UMP2/6-31+G^{**} level. As the electron affinity has a negative value, −15.0 kJ/mol, COF_2 is more stable than COF_2^-. On the other hand, it is also possible that electrons are produced by other temperature-dependent routes, such as electron detachment from CF_3^-, OH^-, or F^-. However, the electron affinities of these ions listed in Table 5 are relatively high; hence, it is difficult to produce electrons, except from COF_2^-. It was confirmed that electrons were produced by electron detachment from COF_2^-.

3.2 O^- + CHF_3 $\rightarrow$ CF_3^- + OH, OH^- + CF_3 (H Abstraction). The fraction of CF_3^- was the largest among the product fractions in the experiment. The CF_3^- + OH channel is expected to proceed by H abstraction of O^-. Figure 9 shows the two complexes on the PES of the CF_3^- + OH channel. The reactant-like complex ($O^-\cdots HCF_3$) with C_{3v} symmetry in Fig. 9(a) is 87.7 kJ/mol lower than the reactants, and the product-like complex ($CF_3^-\cdots$OH) with C_S symmetry in Fig. 9(b) is 108.4 kJ/mol lower than the reactants, as listed in Table 4. Comparing complex 1 with complex 2, the CH bond length in complex 2 is 0.66 Å longer than that in complex 1, as shown in Fig. 9. The atomic charge distribution is also different between these complexes. Although the atomic charge of the O atom in complex 1 is −0.92, the total atomic charge of O and H atoms in complex 2 is only −0.12. This indicates that the electron in the O atom is transferred to CF_3.

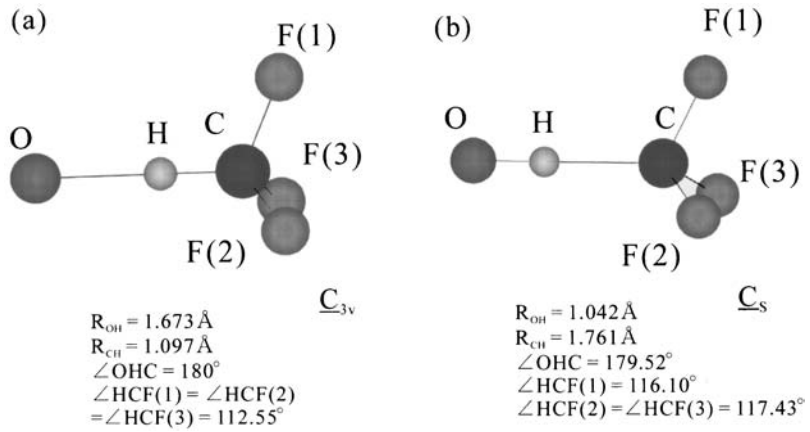

Fig. 9. Geometries of (a) complex 1 and (b) complex 2 of the CF_3^- + OH channel.

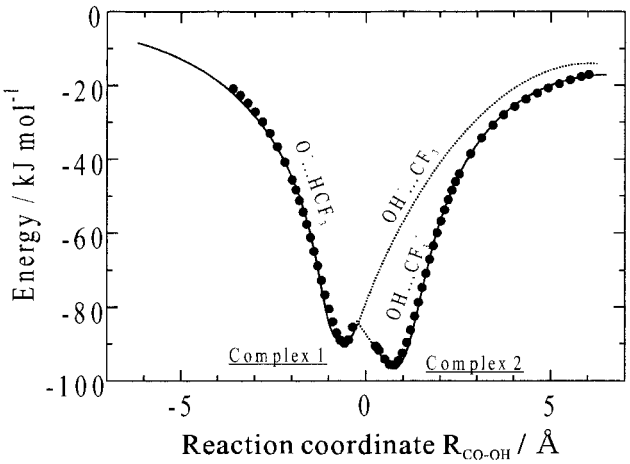

Fig. 10. Schematic diagram of the CF_3^- + OH channel calculated at the UMP2/6-31+G** level.

Figure 10 shows a schematic diagram of the CF_3^- + OH channel obtained at the UMP2/6-31+G** level. The geometries on the $O^-\cdots HCF_3$ surface were optimized in each 0.1 Å (or 0.2 Å) step of the OH bond length, while the geometries on the $CF_3^-\cdots OH$ surface were optimized in each 0.1 Å step of the CH bond length. The zero-point energy calculations are neglected in Fig. 10. The PESs, when the OH bond length is from 1.40 to 1.22 Å, are so complicated that we could not describe the PESs in this region, and no transition state was found in the CF_3^- + OH channel. The PES of $O^-\cdots HCF_3$ is considered to cross that of $OH\cdots CF_3^-$. It is expected that the energy of the crossing point is approximately 80 kJ/mol more exothermic than the reactants, and the OH bond length is near 1.40 Å and the CH bond length is near 1.15 Å according to Fig. 10. Even though the symmetry on the PES of $O^-\cdots HCF_3$ is C_{3v}, the symmetry is considered to be broken to the PES of $OH\cdots CF_3^-$ with C_S symmetry, which is more stable.

The idea of a crossing of the PESs supports the mechanism of the O^- + CH_2F_2 reaction.[24] The crossing of the surfaces also occurs in the H abstraction channel of the O^- + CH_2F_2 reaction. The PES of $OH\cdots CHF_2^-$ crosses the PES of $OH^-\cdots CHF_2$, and the energy of the crossing point is also below that of the reactant. The first excited state of $OH\cdots CHF_2^-$ is $OH^-\cdots CHF_2$ and the PES of the $OH^-\cdots CHF_2$ was calculated to be only about 25.1 kJ/mol higher than the PES of $OH\cdots CHF_2^-$. These results are in good agreement with our calculations.

OH^- was also produced in an experiment.[14] The difference in the reaction enthalpies between the CF_3^- + OH and the OH^- + CF_3 channel is only 5.8 kJ/mol at the MP4(SDTQ)/6-311++G(2df,p)//MP2/6-31+G** level, which explains a possibility for the production of OH^-. It is expected that OH^- is produced by a nonadiabatic transition to the PES of $OH^-\cdots CF_3$, which corresponds to an electric excited state of the $OH\cdots CF_3^-$ PES.

It is concluded that the H abstraction reaction easily proceeds under thermal conditions because there is no reaction barrier in this channel.

3.3 Difference in Reactivity between the O^- + CF_4 and O^- + CHF_3 Reactions. The results of ab initio calculations on the O^- + CF_4 reaction and the O^- + CHF_3 reaction agree with the experimental results. It is very interesting that the difference in the reactivity of O^- with CF_4 and CHF_3 is very large. There is a possibility that the presence of the H atom in the molecule has a large effect on the reactivity. It is worth comparing the reaction O^- + CF_4, CHF_3 with the reaction O^- + CH_2F_2.[24] Product ions from the O^- + CH_2F_2 reaction are e^- (38%), OH^- (25%), CF_2^- (37%), and F^- (< 1%). The reaction proceeds on the $OH\cdots CHF_2^-$ surface at the first step, and the surface is separated into two channels, the $OH^-\cdots CHF_2$ surface and the $H_2O\cdots CF_2^-$ surface. Hence, the O^- + CH_2F_2 reaction proceeds mainly via an H abstraction. In the case of O^- with CF_4, there is no hydrogen abstraction reaction, which is one reason for the low reactivity. Even though it is possible that O^- attacks an F atom nucleophilically, only the S_N2-type reaction channel is considered to exist because the negatively charged F atom repels the negatively charged O anion. Since four negatively charged F atoms surround the C atom (Fig. 11(a)) and repel O^-, it requires a high energy when O^- attacks the C atom nucleophilically. In the case of O^- with CHF_3, the reaction channel of the H abstraction by O^- exists along with the S_N2-type reaction channel. Even though three negatively charged F atoms exist in the molecule shown in Fig. 11(b), the positively charged H atom exists on the edge of the molecule, and it is easier for the O anion to approach the CHF_3

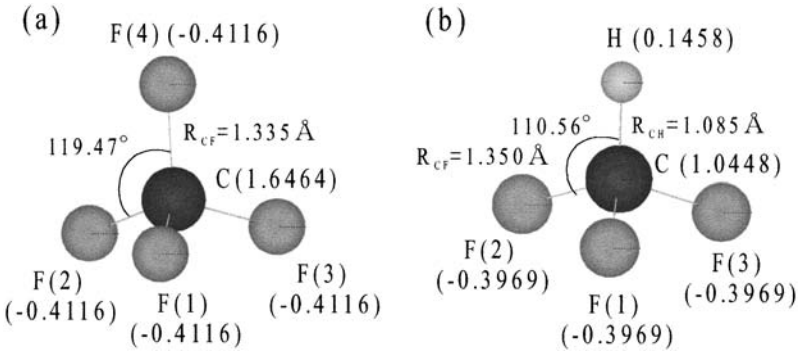

Fig. 11. Geometries and atomic charges of (a) CF_4 and (b) CHF_3 calculated at the RMP2/6-31+G** level.

molecule. As we observed in the case of the $O^- + CHF_3$ reaction, O^- approaches the H atom at the first step in both the H abstraction reaction and the S_N2-type reaction.

Wang et al. reported that fluorine substitution could affect the H abstraction process of the reaction of $O(^3P)$ with fluoromethanes.[15] The barriers for the reactions of $O(^3P)$ with fluoromethanes are 4–21 kJ/mol higher than that of the $O(^3P) + CH_4$ reaction. The $O(^3P) + CHF_3$ reaction possesses the highest barrier, while the $O(^3P) + CH_3F$ and $O(^3P) + CH_2F_2$ reactions involve nearly equal barriers. Wang et al. also mentioned the effect of fluorine substitution on the energy barriers for the reactions of $NH(X^3\Sigma^-)$ with fluoromethanes. When one of the H atoms in CH_4 is substituted by an F atom, the barrier height for the corresponding reaction is reduced. However, the barrier for the $NH + CHF_3$ reaction becomes slightly larger than that for the $NH + CH_4$ reaction. They concluded that this might be caused by the stabilization of trifluoromethyl, which made the CH bond in CHF_3 somewhat stronger than that in CH_4. As mentioned above, previous studies indicated that the effect of fluorine substitution for the fluoromethane reactions was relatively large. According to previous studies, the effect of the substitution of an F atom in CF_4 by an H atom is considered to be rather large. The H atom substitution adds to the important reaction path for the reactivity, the H abstraction channel.

It is concluded that the difference in reactivity between the $O^- + CF_4$ and $O^- + CHF_3$ reactions depends on the difference in the atomic charge distributions between CF_4 and CHF_3, brought about by the H substitution.

Conclusions

We have studied the reactions of O^- with CF_4 and CHF_3 by ab initio molecular orbital calculations. In the case of the $O^- + CF_4$ reaction, only $CF_3O^- + F$, $F^- + CF_3O$, and $F_2^- + CF_2O$ channels were calculated because other channels are endothermic. Even though one transition state geometry was optimized, the activation energy was rather high, approximately 222 kJ/mol calculated at the UMP2/6-31+G** level. The PES branches to three parts at the transition state and produces $CF_3O^- + F$, $F^- + CF_3O$, and $F_2^- + CF_2O$ channels. The large activation energy is in good agreement with the lack of reactivity in the experimental study.

In the case of the $O^- + CHF_3$ reaction, the number of reaction channels increased because the H abstraction channel exists in addition to the S_N2-type reaction. In the S_N2-type reaction, $HF + COF_2^-$ and $HF_2^- + COF$ are produced at the first step. Then, F^-, HF, and COF are produced from each reaction channel. Electrons are also produced from the S_N2-type reaction by electron detachment from COF_2^-. Furthermore, there was no reaction barrier in the S_N2-type reaction. In the H abstraction reaction, $CF_3^- + OH$ and $OH^- + CF_3$ are produced. The PESs cross and no transition state exists.

Comparing the $O^- + CF_4$ reaction with the $O^- + CHF_3$ reaction, the H atom in CHF_3 greatly influences the reactivity. Because of the positively charged H atom, O^- can more easily approach the CHF_3 molecule.

We should like to thank Prof. Mitsuo Koshi, Dr. Tohru Nakajima, and Dr. Masateru Nishioka (The University of Tokyo) for technical support and valuable discussions. This research was supported by JST (Japan Science and Technology Corporation) under the CREST program.

References

1 J. V. Gompel and T. Walling, *Semicond. Int.*, 95 (1995).
2 S. Kanno, S. Ikeda, H. Yamashita, S. Azuhata, K. Irie, and S. Tamata, *Mat. Res. Soc. Sym. Proc.*, **497**, 59 (1998).
3 C. L. Hartz, J. W. Bevan, M. W. Jackson, and B. A. Wofford, *Environ. Sci. Technol.*, **32**, 682 (1998).
4 B. A. Wofford, M. W. Jackson, C. Hartz, and J. W. Bevan, *Environ. Sci. Technol.*, **33**, 1892 (1999).
5 E. E. Ferguson, F. C. Fehsenfeld, and D. L. Albritton, "Gas-Phase Ion chemistry," ed by M. T. Bowers, Academies Press, New York (1979), Vol. 1, Chap. 2.
6 R. P. Wayne, "Chemistry of Atmospheres," 2nd ed, Clarendon Press, Oxford (1991), Chap. 6.
7 A. A. Viggiano, R. A. Morris, F. Dale, and J. F. Paulson, *J. Phys. Chem.*, **93**, 1149 (1990).
8 K. M. Ervin and P. B. Armentrout, *J. Chem. Phys.*, **83**, 166 (1985).
9 R. A. Morris, A. A. Viggiano, and J. F. Paulson, *Int. Rev. Phys. Chem.*, **15**,183 (1996).
10 R. A. Morris, A. A. Viggiano, T. M. Miller, J. V. Seeley, S. T. Arnold, and J. F. Paulson, *J. Phys. Chem.*, **100**, 10641 (1996).
11 R. A. Morris, T. M. Miller, A. A. Viggiano, and J. F. Paulson, *J. Geophys. Res.*, **100**, 1287 (1995).
12 R. A. Morris, *J. Chem. Phys.*, **97**, 2372 (1992).
13 C. A. Mayhew, R. Peverall, and P. Watts, *Int. J. Mass Spectrom. Ion Processes*, **125**, 81 (1993).
14 R. Peverall, R. A. Kennedy, C. A. Mayhew, and P. Watts,

Int. J. Mass Spec. Ion. Processes, **171**, 51 (1997).
15 B. Wang, H. Hou, and Y. Gu, *Chem. Phys.*, **1999**, 201.
16 B. Wang, H. Hue, and Y. Gu, *J. Phys. Chem.*, **103**, 9049 (1999).
17 P. Y. Lien, R. M. You, and W. P. Hu, *J. Phys. Chem. A*, **105**, 2391 (2001).
18 V. I. Sorokin, N. P. Gritsan, and A. I. Chichinin, *J. Chem. Phys.*, **108**, 8995 (1998).
19 B. S. Jursic, *Chem. Phys. Lett.*, **256**, 603 (1998).
20 L. A. Angel and K. M. Ervin, *J. Phys. Chem. A*, **105**, 4042 (2001).
21 M. Igarashi and H. Tachikawa, *Int. J. Mass Spectrom.*, **181**, 151 (1998).
22 S. Irle and K. Morokuma, *J. Chem. Phys.*, **114**, 6119 (2001).
23 A. A. Viggiano, R. A. Morris, T. M. Miller, J. F. Friedman, M. M. Barreto, J. F. Paulson, H. H. Michels, R. H. Hobbs, and J. A. Montgomery, Jr, *J. Chem. Phys.*, **106**, 8455 (1997).
24 E. P. F. Lee and J. M. Dyke, *Mol. Phys.*, **88**, 143 (1996).
25 C. A. Mayhew, R. Peverall, and P. Watts, *Int. J. Mass Spectrom. Ion Processes*, **125**, 81 (1993).
26 E. P. F. Lee, J. M. Dyke, and C. A. Mayhew, *J. Phys. Chem. A*, **102**, 8349 (1998).
27 M. J. Frisch, G. W. Trucks, H. B. Schlegel, G. E. Scuseria, M. A. Robb, J. C. Burant, S. Dapprich, J. M. Millam, A. D. Daniels, K. N. Kudin, M. C. Strain, O. Farkas, J. Tomasi, V. Barone, M. Cossi, R. Cammi, B. Mennucci, C. Pomelli, C. Adamo, S. Clifford, J. Ochterski, G. A. Petersson, P. Y. Ayala, Q. Cui, K. Morokuma, D. K. Malick, A. D. Rabuck, K. Raghavachari, J. B. Foresman, J. Cioslowski, J. V. Ortiz, B. B. Stefanov, G. Liu, A. Liashenko, P. Piskorz, I. Komaromi, R. Gomperts, R. L. Martin, D. J. Fox, T. Keith, M. A. Ai-Laham, C. Y. Peng, A. Nanayakkara, C. Gonzalez, M. Challacombe, P. M. W. Gill, B. Johnson, W. Chen, M. W. Wong, J. L. Andres, M. Head-Gordon, E. S. Replogle, and J. A. Pople, "Gaussian 98 (Revision A. 1)," Gaussian, Inc., Pittsburgh, PA (1998).
28 http://webbook.nist.gov/.
29 R. A. Morris, T. M. Miller, J. F. Paulson, A. A. Viggiano, M. T. Feldmann, R. A. King, and H. F. Schaefer III, *J. Chem. Phys.*, **110**, 8436 (1999).